
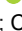













RESEARCH ARTICLE | MARCH 11 2024

Effect of temperature on dislocation-tuned dielectricity and piezoelectricity in single-crystal BaTiO₃

Felix Dietrich ; Fan Ni ; Lovro Fulanović ; Xiandong Zhou  ; Daniel Isaia ;
 Pedro B. Groszewicz ; Chunlin Zhang ; Bai-Xiang Xu ; Jürgen Rödel ; Gerd Buntkowsky ;
 Fangping Zhuo  



Appl. Phys. Lett. 124, 112904 (2024)

<https://doi.org/10.1063/5.0191394>

**Articles You May Be Interested In**

Effect of temperature on domain wall–pore interactions in lead zirconate titanate: A phase-field study

Appl. Phys. Lett. (December 2021)

Observation of dislocation-controlled domain nucleation and domain-wall pinning in single-crystal BaTiO₃

Appl. Phys. Lett. (November 2023)

Second- and Higher-Order Effective Elastic Constants of Cubic Crystals under Hydrostatic Pressure

J. Appl. Phys. (June 1968)

02 June 2025 09:13:25



Applied Physics Letters

**Special Topics Open
for Submissions**

[Learn More](#)

Effect of temperature on dislocation-tuned dielectricity and piezoelectricity in single-crystal BaTiO₃

Cite as: Appl. Phys. Lett. **124**, 112904 (2024); doi: [10.1063/5.0191394](https://doi.org/10.1063/5.0191394)

Submitted: 13 December 2023 · Accepted: 28 February 2024 ·

Published Online: 11 March 2024



View Online



Export Citation



CrossMark

Felix Dietrich,¹ Fan Ni,² Lovro Fulanović,² Xiandong Zhou,^{3,4,a)} Daniel Isaia,² Pedro B. Groszewicz,⁵ Chunlin Zhang,⁶ Bai-Xiang Xu,² Jürgen Rödel,² Gerd Buntkowsky,¹ and Fangping Zhuo^{2,a)}

AFFILIATIONS

¹Institute of Physical Chemistry, Technical University of Darmstadt, 64287 Darmstadt, Germany

²Department of Materials and Earth Sciences, Technical University of Darmstadt, 64287 Darmstadt, Germany

³Failure Mechanics and Engineering Disaster Prevention Key Laboratory of Sichuan Province, College of Architecture and Environment, Sichuan University, Chengdu 610207, China

⁴MOE Key Laboratory of Deep Earth Science and Engineering, College of Architecture and Environment, Sichuan University, Chengdu 610065, China

⁵Department of Radiation Science and Technology, Delft University of Technology, Delft 2629JB, Netherlands

⁶Physcience Optoelectronics Co., Ltd., Beijing 100190, China

^{a)} Authors to whom correspondence should be addressed: xdzhou@scu.edu.cn and zhuo@ceramics.tu-darmstadt.de

ABSTRACT

The pinning-controlled mobility of ferroelectric/ferroelastic domain walls is an important part of managing polarization switching and determining the final properties of ferroelectric and piezoelectric materials. Here, we assess the impact of temperature on dislocation-induced domain wall pinning as well as on dislocation-tuned dielectric and piezoelectric response in barium titanate single crystals. Our solid-state nuclear magnetic resonance spectroscopy results indicate that the entire sample exclusively permits in-plane domains, with their distribution remaining insensitive to temperature changes below the Curie temperature (T_C). The domain wall pinning field monotonically decreases with increasing temperature up to T_C , as evidenced by a combination of experimental observations and phase-field simulations. Our work highlights the promising potential of dislocation engineering in controlling domain wall mobility within bulk ferroelectrics.

© 2024 Author(s). All article content, except where otherwise noted, is licensed under a Creative Commons Attribution (CC BY) license (<https://creativecommons.org/licenses/by/4.0/>). <https://doi.org/10.1063/5.0191394>

Domain wall motion is crucial to the intricate, linear, and nonlinear macroscopic responses of ferroics,^{1–5} a phenomenon enriched by intriguing pinning and depinning dynamics in ferroelectrics and ferromagnets.^{4,5} Defects control can be tuned to alter the dynamics of disordered systems and promise technological relevance (e.g., memory devices). Dislocations are the main carriers of plastic deformation in metals.^{6,7} In ferroelectric ceramics, dislocations facilitate the nucleation of domains and provide local pinning sites for the motion of domain walls^{8–11} due to their associated strain fields and space charge layers surrounding dislocation cores. Ferroelectrics, with their strong coupling between lattice (strain) and charge (polarization) degrees of freedom,¹² provide an ideal platform for examining how dislocations can tune ceramic functionality, which is intrinsically linked to the complex macroscopic responses driven by domain wall motion. In thin-film ferroelectrics, dislocations

have often been considered as a culprit for the degradation of properties.^{13–15} Recently, we reported that the presence of densely packed dislocations in BaTiO₃ single crystals contributes to an immense, 19-fold increase in the converse piezoelectric coefficient.¹⁶ Also, anisotropic electromechanical properties can be designed and dislocation-induced degradation has been eliminated by taking full use of the interactions between dislocations and domain walls.^{17,18} Our prior *in situ* transmission electron microscopy observations have documented pronounced local pinning events that affect domain wall movement throughout both the heating and cooling cycles.^{16,19} While the impact of strains from dislocations and domain walls on functionality depends on their magnitude, orientation, symmetry, and spatial distribution within the material, there is very little macroscopic and detailed information on the influence of temperature on dislocation-associated domain wall pinning.

In this Letter, we investigated the dislocation-related domain wall pinning in single-crystal BaTiO₃. Specifically, we focused on the temperature dependence of the pinning field in experiments and simulations using a phase-field approach. We strategically chose to apply loading along the [110] crystallographic direction of BaTiO₃, aiming to activate the {100}<100> high-temperature slip system. This approach promotes plastic deformation at a substantially lower yield stress, below 100 MPa, as compared to the stress levels encountered with [001] loading.¹⁷ [110]-oriented BaTiO₃ single crystals (coordinate system: X: [110]; Y:[001]; Z:[110], geometry: 4 × 4 × 8 mm³, GK EAST Optoelectronic Technologies, Inc.) were grown using a top-seeded solution method. Uniaxial compression was performed at 1150 °C along the crystallographic [110] direction using a Z010 load frame (Zwick/Roell) equipped with a furnace (HTM Reetz GmbH). Detailed stress-strain curve and experimental setup can be found in Fig. S1 and in our previous reports.^{17,18,20} The dislocation-associated strains are imposed into a ferroelectric tetragonal BaTiO₃ crystal with a parallel configuration between dislocations and 90° domain walls, see schematic in Fig. 1(a).

After mechanical imprint, stripe domain patterns along the [001] direction were observed when compared with domain patterns in the reference sample, see Fig. 1(b) and detailed comparison in Fig. S2. The activated {100}<100> slip systems and dislocation alignment along the [001] direction were confirmed by our previous transmission electron microscopy results.^{10,17} The spatial arrangement of strains originating from {100}<100> dislocations maximizes formation of a₁/a₂ domain walls. Thus, it facilitates an in-depth analysis of the controlled domain nucleation process and the intricate interactions between dislocation strain fields and ferroelastic 90° domain walls. This configuration plays a pivotal role in shaping the dielectric and piezoelectric properties of BaTiO₃. Deformed crystals were cut into smaller pieces (~4 × 4 × 1 mm³) with the two large surfaces normal to the [110] using a Model 4240 Benchtop (Well Diamantdrahtsäge GmbH). The as-prepared [110]-oriented samples were further validated via a Model 1001 Laue backreflection (Huber, Rimsting), achieving an orientation accuracy of ±0.5°. Gold electrodes were sputtered onto the two larger surfaces of both the deformed and reference samples for electrical

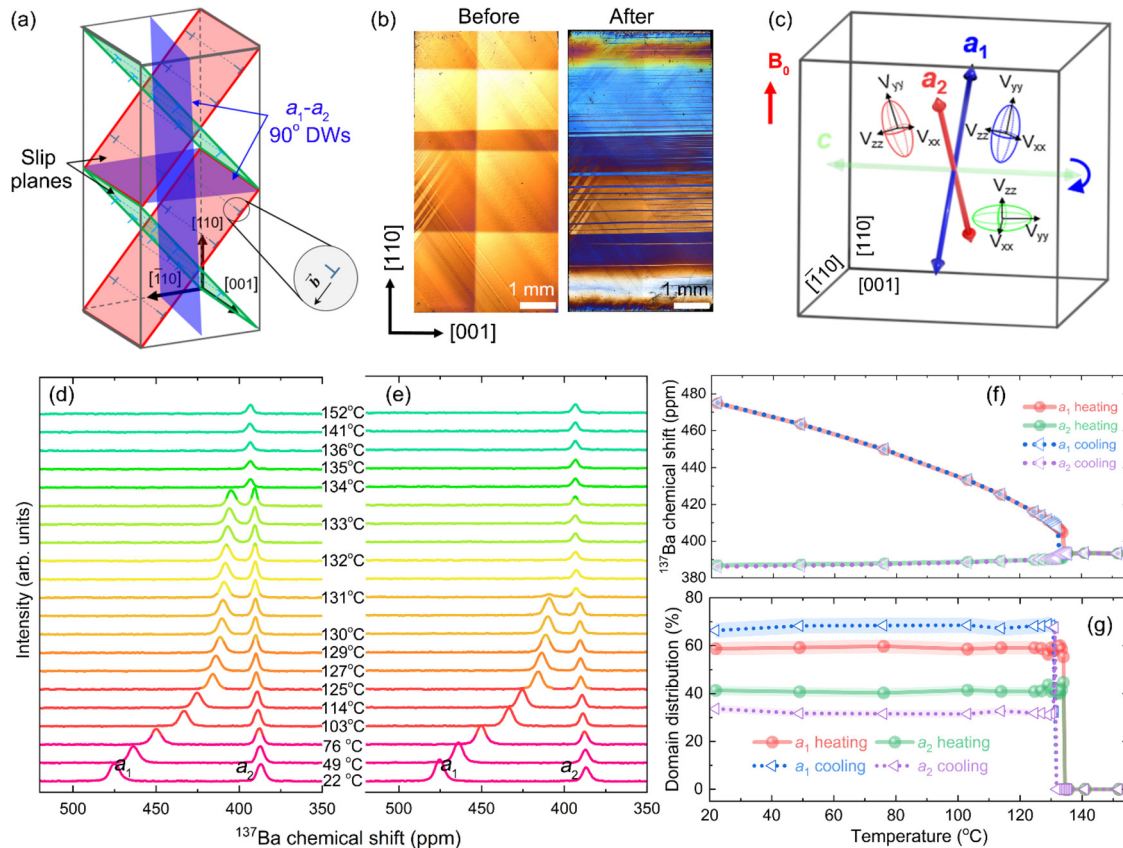


FIG. 1. (a) Schematic featuring the slip planes of the {100}<100> slip systems and permissible a₁-a₂ 90° domain walls (DWs). (b) The aligned dislocations by mechanical imprint altered the macroscopic domain structures. All optical images were captured using a 3D laser-scanning microscope (LEXT OLS4100, Olympus), employing differential interference contrast (DIC) and stitching modes to effectively visualize the domain structures. It should be noted that in stitching mode, horizontal and vertical lines may manifest along the edges of the images. These uniformly distributed lines should not be confused with the domain structure illustrated in Fig. 1(b). (c) The orientations of the spontaneous polarization vectors are denoted with three different ellipsoids (red, blue, and green). The orientation of the electric field gradient tensor at the barium site for different domain (a₁, a₂, and c) orientations of the spontaneous polarization are indicated with three different ellipsoids (red, blue, and green), which represent a₂, a₁, and c polarization vectors. ¹³⁷Ba NMR spectra of the investigated [110]-oriented deformed BaTiO₃ samples: (d) the poled sample during heating and (e) the annealed/unpoled sample during cooling. The annealing was performed at 200 °C for 4 h. (f) ¹³⁷Ba chemical shift and (g) domain distribution during heating and cooling processes.

characterization. All prepared samples were subjected to an annealing process at 200 °C for 4 h to alleviate the residual strain incurred during the cutting and polishing processes.

The mechanical imprint is macroscopically manifested in a modified structure of the domains. To further elucidate the types and distribution of domains, as well as the impact of temperature on domain distribution, we quantified the temperature dependence using the solid-state nuclear magnetic resonance (NMR) spectroscopy. NMR spectra of ^{137}Ba in the deformed sample were recorded using a spectrometer (Bruker Avance III HD) equipped with a wide bore magnet (14.1 T, Oxford). The NMR measurements were conducted with a single-axis goniometer NMR probe (NMR Service GmbH), featuring a nominal resolution of 0.1° and operating at 66.71 MHz. The goniometer probe is connected to a variable temperature control system, enabling a temperature range from −55 to 160 °C. We acquired the NMR spectra by orienting a (110) crystal face at a 50° angle (see schematics in Fig. S3). An angle of 0° signifies that the normal vector of the sample holder is parallel to the magnetic field B_0 . The detailed parameters for the NMR measurements were documented elsewhere.^{10,16,17} The chemical shift of ^{137}Ba is referenced relative to a 1 M solution of BaCl_2 , which is assigned a chemical shift of 0 ppm. The NMR frequency, which directly correlates with the direction of spontaneous polarization vectors, is determined by the orientation of the electric field gradient tensor at the barium sites within different domains,^{16,17,21,22} see Fig. 1(c). Our NMR data revealed that only a_1 and a_2 domains are permissible in the entire sample after direct current poling (1 kV/mm for 10 min) at room temperature [see Fig. 1(d)]. This conclusion was further validated when we rotated the sample from 0° to 60°, observing exclusively a_1 and a_2 domains (see NMR data in Fig. S4). During the heating process, ^{137}Ba chemical shift for a_1 domains decreased and that for a_2 domains slightly increased [Figs. 1(d) and 1(e)], indicating the change in lattice parameters.²³ With further increasing the temperature above the Curie temperature ($T_C = 134$ °C), two NMR peaks for a_1 and a_2 domains merged into one peak due to the phase transition from tetragonal to cubic, in correlation to our temperature-dependent dielectric properties in Fig. S5. In this particular orientation of the single crystal, the ^{137}Ba frequency for the orientation of a_2 domains coincides with the isotropic value of the chemical shift for BaTiO_3 . During heating, the ^{137}Ba resonances assigned to domain orientation a_1 increasingly approach the frequency of the peak assigned to a_2 , until they both collapse at a single resonance at the position of the isotropic chemical shift for BaTiO_3 . The gradual change in position of resonance a_1 is related to the decreasing magnitude of the quadrupolar coupling at the smaller ionic displacements upon approaching a cubic point symmetry above T_C . During the cooling process, these two NMR signals for a_1 and a_2 domains reappeared when temperature was below the Curie temperature (131 °C). With further cooling down to room temperature, a clear separation of NMR signals between a_1 and a_2 domains was identified [Figs. 1(e) and 1(f)]. It is noted that the a_1/a_2 domain ratio during heating is $\sim 60/40$, while the ratio is $\sim 70/30$ during cooling [see Fig. 1(g)]. Poling along the [110] direction slightly increased the amount of a_2 domains.

The slanted polarization-electric field hysteresis loop, reduced spontaneous polarization, and enhanced coercive field (E_c , Fig. S6) highlight the substantial impact of mechanical dislocation imprint on large-signal (super-coercive fields) properties. Our comprehensive study on the effect of introduced dislocations on the high and low field behavior of BaTiO_3 across varied electric fields revealed a marked elevation in the

coercive field as well as enhanced degree of back-switching, as illustrated in Fig. S7, signifying the substantial impact of domain-wall pinning.¹⁶ The full picture of the influence of dislocations on dielectric and piezoelectric properties was achieved within the subcoercive field regime. Our detailed setup for simultaneously quantifying the dielectric and piezoelectric properties at different temperatures is shown in Fig. S8. At 20 °C, the deformed sample in the poled state experienced a substantial rise in relative dielectric permittivity (ϵ_{33}) [see Fig. 2(b)] when the electric field surpassed the pinning field ($E_{\text{pin}} = 16$ V/mm), indicating the activation of dislocation–domain wall interactions. Additionally, a maximum converse piezoelectric coefficient (d_{33}^*) of 2300 pm/V was obtained at 50 V/mm [Fig. 2(b)]. Note that the maximum applied field is $0.25E_c$ for the deformed sample. As demonstrated in Fig. S9, the sharp increase in dielectric loss may contribute to the temperature change of the deformed sample, leading to a large thermal expansion. In general, the corresponding piezoelectric coefficient attributable to thermal expansion can be evaluated as²⁴

$$d_{33}^* = \frac{\beta(T) \times \Delta T \times L}{V}, \quad (1)$$

where $\beta(T)$ is the temperature-dependent coefficient of thermal expansion, ΔT is the temperature change, L is the length or thickness of the sample, and V is the magnitude of the applied AC voltage, respectively. We took the thermal expansion coefficient of 6×10^{-6} K for BaTiO_3 (Ref. 25) and $\Delta T = 1.26$ °C (see the measured temperature change by an infrared camera in Fig. S10). The thermal expansion-induced d_{33}^* was determined to be 15.1 pm/V, which accounts for 1.1% of the measured d_{33}^* of the deformed sample. Therefore, it is reasonable to conclude that the significant piezoresponse observed in the deformed sample is attributed to the interactions between dislocations and domain walls. Upon heating up to T_C , the maximum ϵ_{33} and d_{33}^* reached 27 800 and 2800 pm/V, respectively, when the temperature approached 120 °C. As the temperature was raised above T_C , d_{33}^* value diminished, and ϵ_{33} remained constant, indicating the absence of domain wall pinning under the application of an electric field.

To corroborate the experimentally observed piezoelectric response and shed light on the underlying mechanism, we conducted phase-field simulations^{16,26} and utilized the generalized theory of configurational forces.^{27,28} A set of fundamental equations governs the complex electro-mechanical behavior of ferroelectrics: the mechanical stress equilibrium equation, Gauss's law, and the time-dependent Ginzburg–Landau equation,¹⁷

$$\sigma_{ij,j} = 0, D_{i,i} - q = 0, \dot{P}_i = -M \frac{\delta f}{\delta P_i}, \quad (2)$$

where σ_{ij} is the stress, D_i is the electric displacement field, q is the volume charge density, P_i is the electric polarization, and M is the mobility parameter, respectively. The total free energy density of the BaTiO_3 single crystal is given as^{16,17}

$$\begin{aligned} f = & \alpha_{ij} P_i P_j + \alpha_{ijkl} P_i P_j P_k P_l + \alpha_{ijklmn} P_i P_j P_k P_l P_m P_n \\ & + \alpha_{ijklmnpq} P_i P_j P_k P_l P_m P_n P_p P_q \\ & + \frac{1}{2} c_{ijkl} (\epsilon_{ij} - \epsilon_{ij}^P - \epsilon_{ij}^D) (\epsilon_{kl} - \epsilon_{kl}^P - \epsilon_{kl}^D) \\ & - \frac{1}{2} \kappa_0 \kappa_{ij} E_i E_j - P_i E_i + \frac{1}{2} g_{ijkl} P_i P_j P_k P_l, \end{aligned} \quad (3)$$

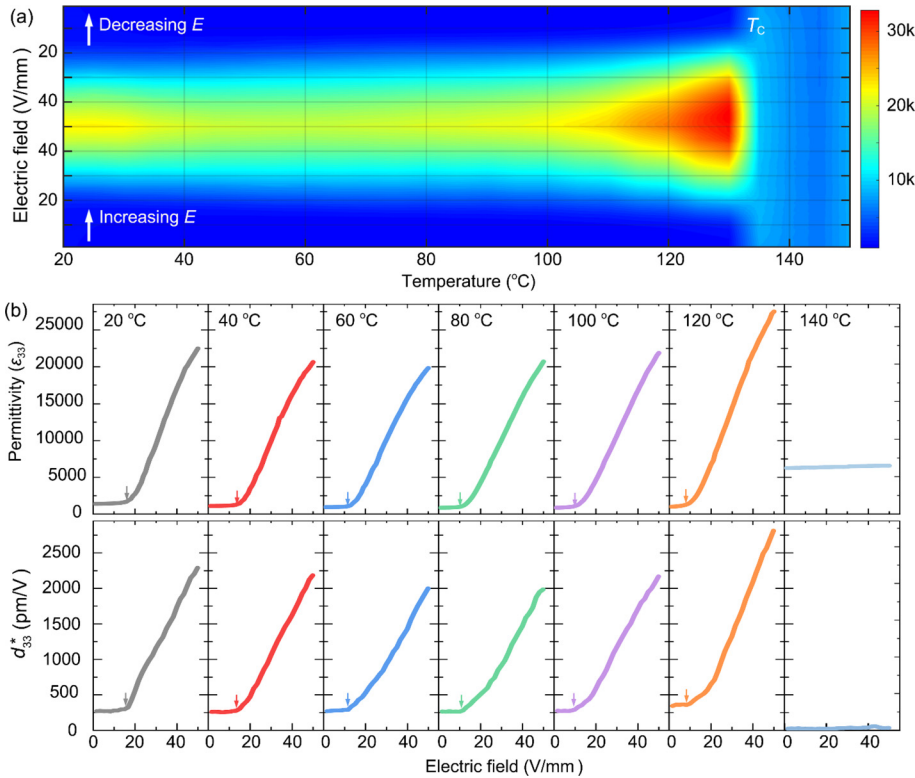


FIG. 2. (a) Relative dielectric permittivity (ϵ_{33}) map in the AC field-temperature space. (b) Permittivity (ϵ_{33}) and corresponding converse piezoelectric coefficient (d_{33}^*) of the deformed sample quantified at different temperatures with a frequency of 1 kHz. Note that the solid arrows indicate the positions of the pinning fields.

where α_{ij} , α_{ijkl} , α_{ijklmn} , and $\alpha_{ijklmnpq}$ are the Landau coefficients. Only α_{ij} are linearly dependent on temperature. c_{ijkl} are the elastic stiffness tensors, $\epsilon_{ij} = (u_{i,j} + u_{j,i})/2$ is the total strain defined as the symmetric part of the displacement gradient $u_{i,j}$. $\epsilon_{ij}^p = Q_{ijkl}P_kP_l$ is the eigenstrain induced by polarization, and Q_{ijkl} are the electrostrictive coefficients. ϵ_{ij}^D is the eigenstrain of dislocations formulated based on a nonsingular continuum theory of dislocations.¹⁶ κ_0 and κ_{ij} are the dielectric permittivity of the vacuum and the relative dielectric permittivity of the background of the bulk, respectively. E_i is the electric field and g_{ijkl} are the gradient energy coefficients. In the finite element simulations, the driving force is calculated in the postprocessing as¹⁷

$$F_k = - \sum_{I=1}^{n_{nod}} \bigcup_{e=1}^{n_{el}} \int_{V_e} \Sigma_{kj} N_j^I dV, \quad (4)$$

where the assembly operation U is performed over n_{el} elements adjacent to node I , the summary operation Σ is performed over n_{nod} in the integration domain, V_e is the volume of the element, and N_j^I is the gradient of the shape function in the finite element method. Σ_{kj} is the generalized Eshelby stress tensor for coupled electromechanical problems in ferroelectrics.^{10,17} Considering the multi-slip structures of dislocation with perpendicular Burgers vectors in the high-temperature plastic deformation, we incorporated a simple dislocation network consisting of an a_1/a_2 90° domain wall and four dislocations with perpendicular Burgers vectors along the [100] and [010] directions [Fig. 3(a)]. This approach allowed us to calculate the potential energy (U) of the domain wall,^{17,25,29}

$$U = - \int_0^L F_1 dx_1, \quad (5)$$

where L is the position of the domain wall in the horizontal directions as shown in Fig. 3(a) and F_1 is the local pinning force on the domain wall along the x_1 direction (perpendicular to the domain wall). Note that the fully coupled governing equations are simultaneously solved in the simulation, which takes into account the influence of dislocation-induced nucleation of new domains on the driving force of domain walls.²⁷ The material parameters can be found in Table S1. Our phase-field model is numerically implemented using the finite element method within the simulator “Panda’s Multi-Physics” (PMP) developed based on the open-source software Multiphysics Object-Oriented Simulation Environment (MOOSE) framework.³⁰

The domain wall underwent bulging or straightening as it encountered a dislocation pair, with the associated driving force depicted in Fig. 3(b) at $0.24T_C$. This pair of dislocations, with perpendicular Burgers vectors, generated antisymmetric pinning forces that effectively pinned the domain wall during AC field cycling. In the corresponding potential energy profile [Figs. 3(c) and 3(d)], two energy minima indicate stable equilibrium positions for the domain wall. This implies that a pinning field is required to overcome the local energy barriers. The presence of two equilibrium positions enabled the domain wall to develop reversible and irreversible displacements between these positions, resulting in a high electric field-dependent electromechanical response.³¹ It is worth noting that as long as the dislocation network was introduced into a bulk ferroelectric, the pinning force profile and energy landscape induced by dislocations were

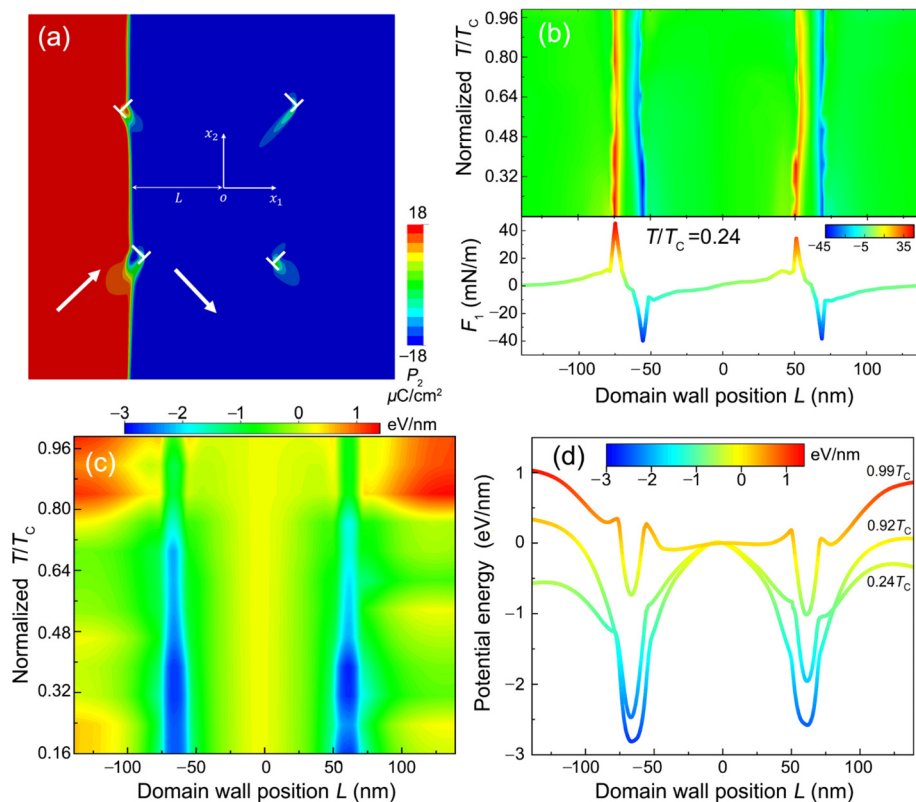


FIG. 3. (a) Schematic of the phase-field model with a size of $300 \times 300 \text{ nm}^2$. The periodic boundary condition is applied for top and bottom surfaces. The left and right surfaces are traction-free, and the applied surface charge density is consistent with P_1 . (b) Calculated driving force (F_1) map and (c) potential energy in the temperature-domain wall position space. (d) Selected potential energy profiles at different temperatures below T_C .

formed and presented possible barriers for domain walls. Consequently, strong interactions between dislocations and domain walls can be experimentally achieved in poled deformed samples.

Such interactions can be maintained up to T_C and then vanish with further temperature increases above T_C . As the temperature increased, the local energy barriers exhibited a decrease, leading to the reduced pinning field (see our measured and simulated results in Fig. S11). Our simulations of the pinning field, which account for contributions from both 90° and 180° domain walls, align well with the observed temperature-dependent trends in the experimentally quantified pinning field (see Fig. S11). Above $0.88T_C$ [Fig. 3(c)], the domain wall started to exhibit metastable equilibrium positions characterized by shallow energy potential wells. At $0.99T_C$, six potential energy wells can be observed [Fig. 3(d)]. Our calculations suggest the presence of a greater number of reversible and irreversible displacements for the domain wall, leading to a higher electromechanical response at elevated temperatures. We note that the potential energy profile with respect to the domain wall position at temperature close to T_C had a small curvature (so-called flat energy profile^{32–34}) consequently leading to a high piezoelectric coefficient.³² Our calculations revealed that the total free energy of the system is predominantly influenced by variations in the electric energy concerning the domain wall position at different temperatures (see Fig. S12). Above T_C , the domain walls vanished, and hence lacked the option for domain wall pinning. This phenomenon aligns well with our experimental observation of the absence of a pinning field, as depicted in Fig. 2(b). While we cannot entirely exclude the possibility that local domain switching contributes

to dielectric and piezoelectric responses, such contributions are likely not predominant. Our simulations and experimental observations support this conclusion, which consistently revealed a stable domain ratio across various temperatures.

In summary, a “forest” of well-selected dislocations with the $\{100\}\{100\}$ slip systems were created in barium titanate single crystals via high-temperature uniaxial compression along the $[110]$ direction. We found that the imprinted dislocations oriented in the out-of-plane $[001]$ direction favored in-plane a_1 and a_2 domains, and the a_1/a_2 domain ratio was insensitive to the temperature change below the Curie temperature. By experimental observations and phase-field simulations, it is documented that domain-wall pinning field by dislocations decreased with increasing temperature up to the Curie temperature. Our calculations of the potential energy profile and driving force elucidated the temperature-dependent behavior observed in the dislocation-tuned dielectric and piezoelectric properties. Our work introduces an additional control mechanism for ferroelectric materials, where temperature acts as a variable to regulate the dislocation-based motion and functionality of domain walls.

See the supplementary material for high-temperature plastic deformation experiment, optical images, and electrical properties, and phase-field simulations.

We thank Professor Dragan Damjanovic for helpful discussions. We thank Professor Karsten Durst for access to the laser scanning microscope. This work was supported by the German Research

Foundation (DFG) through Project Nos. 414179371 and 530438323. The simulation work was partially funded through Project No. 398072825 of DFG. P.B.G. acknowledges financial support by the Dutch Research Council (NWO) for the ECCM Tenure Track funding under Project No. ECCM.006. P.B.G. and G.B. acknowledge funding under DFG Contract Bu-911-28-1. G.B. acknowledges funding from the DFG under Contract Bu-911-28-2. X.Z. acknowledges support from the National Natural Science Foundation of China (No. 12302231), the Sichuan Science and Technology Program (No. 2023NSFSC0910), the China Postdoctoral Science Foundation (No. 2023M732433), and the Fundamental Research Funds for the Central Universities in China (No. 2023SCU12103). F.Z. acknowledges the Alexander von Humboldt Foundation for the fellowship with Award No. 1203828.

AUTHOR DECLARATIONS

Conflict of Interest

The authors have no conflicts to disclose.

Author Contributions

Felix Dietrich: Conceptualization (equal); Data curation (equal); Formal analysis (equal); Investigation (equal); Methodology (equal); Validation (equal); Visualization (equal); Writing – original draft (supporting); Writing – review & editing (equal). **Fan Ni:** Formal analysis (equal); Investigation (equal); Visualization (equal); Writing – review & editing (equal). **Lovro Fulanovic:** Data curation (equal); Formal analysis (equal); Investigation (equal); Visualization (equal); Writing – review & editing (equal). **Xiandong Zhou:** Conceptualization (equal); Data curation (equal); Funding acquisition (equal); Methodology (equal); Software (equal); Validation (equal); Writing – original draft (supporting); Writing – review & editing (equal). **Daniel Isaia:** Investigation (equal); Methodology (equal); Visualization (equal); Writing – review & editing (equal). **Pedro B. Groszewicz:** Data curation (equal); Formal analysis (equal); Funding acquisition (equal); Methodology (equal); Validation (equal); Writing – review & editing (equal). **Chunlin Zhang:** Data curation (equal); Formal analysis (equal); Methodology (equal); Writing – review & editing (equal). **Bai-Xiang Xu:** Data curation (equal); Formal analysis (equal); Funding acquisition (equal); Methodology (equal); Software (equal); Writing – review & editing (equal). **Jürgen Rödel:** Conceptualization (equal); Funding acquisition (equal); Methodology (equal); Project administration (equal); Supervision (equal); Validation (equal); Writing – original draft (supporting); Writing – review & editing (equal). **Gerd Buntkowsky:** Conceptualization (equal); Data curation (equal); Funding acquisition (equal); Methodology (equal); Project administration (equal); Supervision (equal); Validation (equal); Writing – original draft (supporting); Writing – review & editing (equal). **Fangping Zhuo:** Conceptualization (equal); Data curation (equal); Funding acquisition (equal); Investigation (equal); Methodology (equal); Validation (equal); Visualization (equal); Writing – original draft (lead); Writing – review & editing (equal).

DATA AVAILABILITY

The data that support the findings of this study are available from the corresponding authors upon reasonable request. Source codes of MOOSE-based application PMP are available in the online repository: bitbucket.org/pandasmultiphysics/pmp/wiki/Home (Ref. 35).

REFERENCES

- T. J. Yang, V. Gopalan, P. J. Swart, and U. Mohideen, *Phys. Rev. Lett.* **82**, 4106 (1999).
- H. H. Wu, J. Wang, S. G. Cao, and T. Y. Zhang, *Appl. Phys. Lett.* **102**, 232904 (2013).
- D. M. Juraschek, Q. N. Meier, M. Trassin, S. E. Trolier-McKinstry, C. L. Degen, and N. A. Spaldin, *Phys. Rev. Lett.* **123**, 127601 (2019).
- T. Koyama, D. Chiba, K. Ueda, K. Kondou, H. Tanigawa, S. Fukami, T. Suzuki, N. Ohshima, N. Ishiwata, Y. Nakatani, K. Kobayashi, and T. Ono, *Nat. Mater.* **10**, 194 (2011).
- M. Duerschnebel, M. Yi, K. Uestuener, M. Liesegang, M. Katter, H.-J. Kleebe, B. Xu, O. Gutfleisch, and L. Molina-Luna, *Nat. Commun.* **8**, 54 (2017).
- P. M. Anderson, J. P. Hirth, and J. Lothe, *Theory of Dislocation* (Cambridge University Press, New York, 2017).
- U. Messerschmidt, *Dislocation Dynamics During Plastic Deformation* (Springer, Berlin, Heidelberg, 2010).
- H. H. Wu, J. Wang, S. G. Cao, and T. Y. Zhang, *J. Appl. Phys.* **114**, 164108 (2013).
- S. Y. Hu, Y. L. Li, and L. Q. Chen, *J. Appl. Phys.* **94**, 2542 (2003).
- F. Zhuo, X. Zhou, S. Gao, F. Dietrich, P. B. Groszewicz, L. Fulanović, P. Breckner, B.-X. Xu, H.-J. Kleebe, D. Damjanovic, and J. Rödel, *Phys. Rev. Lett.* **131**, 016801 (2023).
- L. Cheng, H. Zhang, R. Xu, K. Co, N. Guiblin, M. Otonicar, C. Paillard, Y. Wang, and B. Dkhil, *Appl. Phys. Lett.* **123**, 201903 (2023).
- J. Feng, X. Qian, C.-W. Huang, and J. Li, *Nat. Photonics* **6**, 866 (2012).
- S. P. Alpay, I. B. Misirlioglu, V. Nagarajan, and R. Ramesh, *Appl. Phys. Lett.* **85**, 2044 (2004).
- I. B. Misirlioglu, A. L. Vasiliev, M. Aindow, and S. P. Alpay, *Integr. Ferroelectr.* **71**, 67 (2005).
- M.-W. Chu, I. Szafraniak, R. Scholz, C. Harnagea, D. Hesse, M. Alexe, and U. Göseleg, *Nat. Mater.* **3**, 87 (2004).
- M. Höfling, X. Zhou, L. M. Riemer, E. Bruder, B. Liu, L. Zhou, P. B. Groszewicz, F. Zhuo, B.-X. Xu, K. Durst, X. Tan, D. Damjanovic, J. Koruza, and J. Rödel, *Science* **372**, 961 (2021).
- F. Zhuo, X. Zhou, S. Gao, M. Höfling, F. Dietrich, P. B. Groszewicz, L. Fulanović, P. Breckner, A. Wohninsland, B.-X. Xu, H.-J. Kleebe, X. Tan, J. Koruza, D. Damjanovic, and J. Rödel, *Nat. Commun.* **13**, 6676 (2022).
- F. Zhuo and J. Rödel, *Appl. Phys. Lett.* **122**, 112901 (2023).
- T. Jiang, F. Ni, O. Recalde-Benitez, P. Breckner, L. Molina-Luna, F. Zhuo, and J. Rödel, *Appl. Phys. Lett.* **123**, 202901 (2023).
- M. Höfling, L. Porz, M. Scherer, S. Gao, F. Zhuo, D. Isaia, and J. Rödel, *J. Mater. Sci.* **37**, 737 (2022).
- O. Liechti and R. Kind, *J. Magn. Reson.* **85**, 480 (1989).
- P. B. Groszewicz, *Open Ceram.* **5**, 100083 (2021).
- M. K. Lee, T. K. Nath, C. B. Eom, M. C. Smoak, and F. Tsui, *Appl. Phys. Lett.* **77**, 3547 (2000).
- D. Wang, Y. Fotinich, and G. P. Carman, *J. Appl. Phys.* **83**, 5342 (1998).
- G. Shirane and A. Takeda, *J. Phys. Soc. Jpn.* **7**(1), 1–4 (1952).
- X. Zhou, C. Reimuth, and B.-X. Xu, *Int. J. Solids Struct.* **249**, 111688 (2022).
- X. Zhou, Z. Liu, and B.-X. Xu, *Int. J. Solids Struct.* **238**, 111391 (2022).
- W. Cai, A. Arsenlis, C. R. Weinberger, and V. V. Bulatov, *J. Mech. Phys. Solids* **54**, 561 (2006).
- X. Zhou, C. Reimuth, P. Stein, and B.-X. Xu, *Arch. Appl. Mech.* **91**, 4499 (2021).
- C. J. Permann, D. R. Gaston, D. Andrés, R. W. Carlsen, F. Kong, A. D. Lindsay, J. M. Miller, J. W. Peterson, A. E. Slaughter, R. H. Stogner, and R. C. Martineau, *SoftwareX* **11**, 100430 (2020).
- D. Damjanovic, *J. Appl. Phys.* **82**, 1788 (1997).
- D. Damjanovic, *Appl. Phys. Lett.* **97**, 062906 (2010).
- F. Li, Z. Lin, Z. Chen, Z. Cheng, J. Wang, C. Li, X. Xu, Q. Huang, X. Liao, L. Q. Chen, T. R. ShROUT, and S. Zhang, *Nat. Mater.* **17**, 349 (2018).
- M. Budimir, D. Damjanovic, and N. Setter, *Phys. Rev. B* **73**, 174106 (2006).
- X. Zhou (2023). “Panda’s Multi-Physics (PMP),” Bitbuckets repository. <https://PandasMultiPhysics@bitbucket.org/pandasmultiphysics/pmp.git>